Modeling of a turbine bladerow with stagger angle variation using the multi-fidelity influence superposition method

H. M. Phan[1]

Department of Engineering Science, University of Oxford, Oxford, United Kingdom

Acknowledgement

The support from the EPSRC CDT in Gas Turbine Aerodynamics and the Chair of Computational Aerothermal Engineering Bursary are much appreciated. The author would like to thank Prof. Li He for his continuous support and Dr. Penghao Duan for the fruitful discussion on the loss analyses. The author would like to thank the anonymous reviewers who gave useful comments for the work. The author would like to acknowledge the use of the University of Oxford Advanced Research Computing (ARC) facility in carrying out this work (http://dx.doi.org/10.5281-/zenodo.22558).

[1] Corresponding author. E-mail address: hien.phan@eng.ox.ac.uk

Modeling of a turbine bladerow with stagger angle variation using the multi-fidelity influence superposition method

ABSTRACT

Manufacturing variabilities can significantly affect a turbine bladerow's performance. With the push for turbine's efficiency and reliability more than ever, the understanding of manufacturing variability impacts is sought after. It has been shown that a multi-passage simulation domain is required to capture the interaction among varied blades. This is a challenge for conventional single-passage methods, largely due to the requirement of prohibitive computational resources. The present work introduces an attempt to solve this challenge by combining the multi-fidelity method and the influence superposition approach. The proposed methodology combines the accuracy of a high-fidelity simulation and the speed of a low-fidelity simulation. Therefore, the multi-fidelity predictions tend to be both accurate and fast. The key enabler is that only a small set of configurations is needed to pre-compute the source term. Two representative geometries of a subsonic low-pressure turbine and a transonic high-pressure turbine have been chosen as the test cases. Each test case is subject to two further stagger angle variation patterns, namely alternating and sinusoidal pattern. The low-fidelity method has been shown to be inadequate for the transonic high-pressure turbine test case, owning to its incapability to capture correctly the

shockwave formation and the shockwave/wake interaction. On the other hand, the proposed multi-fidelity method has been successful to match qualitatively and quantitatively compared to the direct high-fidelity solution. More interestingly, the multi-fidelity method has a reduced computational overhead of one order of magnitude compared to the direct high-fidelity simulation. With an ability to accurately and efficiently predict the manufacturing variability effects, this method provides a tool for engineers to explore and optimize their blading designs.

Keywords: Turbomachinery, Manufacturing variations, Mis-staggering, Multi-fidelity method.

1. Introduction

Aerodynamic design of turbomachinery blades contribute significantly to the machine's efficiency and reliability. It is the current industrial standard to design turbomachinery blades using computational tools such as Computational Fluid Dynamics (CFD) to meet the aerodynamic as well as other structural requirements. Thanks to the cyclic periodicity of a turbomachinery bladerow, it is possible to perform a single-passage Reynolds-Averaged Navier-Stokes (RANS) simulation to estimate the bladerow aerodynamic performance. Unfortunately, there exist inherent variations of the turbomachinery blades in practice, which breaks down the periodicity assumption. These unintended variations change the performance of the design-intent blades. The variations may have several originalities. It may come from the manufacturing processes. Despite the cutting-edge manufacturing techniques and facilities, the finished parts still have

variabilities to some degrees. Controlling a tight tolerance is still unable to remove this source of uncertainty. The variations can also come during the blades' service such as wear and tear or even foreign-object damage.

There have been some past researches in the public domain that examine the effects of these variations on both compressor and turbine blades. Xia et al. [1] investigated the effects of flow and geometric variations on a turbine blade. They found that the variations cause a large drop of the adiabatic efficiency. Wang and Zou [2] studied the impacts of geometric variations on a low-pressure turbine. They pointed out that the mean total pressure loss increases by 2.3% and the wake mixing loss variations were responsible for the performance degradation. Yang et al. [3] examined the effects of blade thickening in a multi-stage steam turbine. They found that the variations affected both the mass flow rate and the total-to-static efficiency and the 1st stage stator blade is the most sensitive region. Voigt et al. [4] examined the effects geometric uncertainties of a representative nozzle guide vane. They concluded that the stagger angle variation had the biggest impact, while the profiled endwall variation had a negligible influence. Lee et al. [5] assessed the performance of high-pressure turbine rotor blades under manufacturing variabilities. They found that the mean exit flow angle was lowered by 0.250, the mean capacity was increased by 0.3%, and the mean efficiency was reduced by 0.8. More importantly, they proved that the multi-passage CFD model is required since the averaging of single-passage models is not reliable. Regarding the compressor blade, Lejon et al. [6] studied the impacts of geometric variations of a rotor blade. They found that both mass flow and total pressure ratio were influenced by the mean shift in geometry. Interestingly, they observed that the impact of one varied blade can be analyzed using a reduced simulation domain that

contains the varied blade itself and some of its adjacent blades rather than simulating an entire blisk. Phan and He [7] investigated the effects of mis-staggering of the compressor bladerow subject to both clean flow and inlet distortion. They found that the mean blade loading was changed up to 20% for the clean flow configuration. Mis-staggering changes the blade unsteady responses [7] and in some particular cases can promote unstable vibration leading to potential catastrophic failures [8]. Lange et al. [9] studied the impacts of manufacturing variabilities on a high-pressure compressor stage performance. They observed that the scatter range of isentropic efficiency can be amplified up to 106% or reduced to 13% compared to the single-passage result depending on the number of passages used in the calculation model. Their observation suggested that the multi-passage calculation is required in the investigation of manufacturing variations. In addition, distortions from intake geometry [10, 11] and upstream wake [7, 12, 13] would also interact with the varied blade to create extra complications.

Another important aspect of interest is the modeling fidelity required to examine the variation effects. Lee et al. [14] compared a variety of modeling fidelity to capture the variation effects. They found that the RANS multi-passage model is required if the stage loading and efficiency needs to be accurately captured. An accurate prediction of the multi-passage bladerow performance could improve the optimized design [15, 16] as well as reducing the scrap rate [17]. Unfortunately, direct high-fidelity RANS computations of many varied multi-passage configurations are prohibitively expensive. A large number of past researches used reduced-order modeling such as polynomial-chaos and Monte-Carlo approaches [1, 2, 4]. Nevertheless, similarly to many other data-driven methods, these methods' accuracy depends heavily on the number and quality of input data. Another

efficient method that can be used for blade variabilities investigation is the spatial Fourier-based method [18, 19]. This method aims to represent the flow field solution of the blade variabilities as a Fourier series. Thus, the truncated harmonic flow solution can be solved for, which is less expensive than a full model. This method is sensitive to the choice of chosen harmonics. For a complicated flow field where a large number of harmonics is required, the efficiency of this method is reduced.

With the background of issues and interests introduced so far, it is clear that we need to have an efficient and accurate method that can capture the multi-passage bladerow performance with manufacturing variations. In the present paper, we introduce the multi-fidelity approach combined with the influence superposition method (ISM) in an attempt to tackle this challenge. The multi-fidelity approach aims to establish a relationship between a low-fidelity and a high-fidelity simulation for the same bladerow geometry and setup. The objective is to be able to predict a high-fidelity solution with computing resources comparable to a low-fidelity simulation. On the other hand, the influence superposition method is the physics-based method that aims to estimate the effects of blade variations by superimposing each individual blade's contribution. This is based on the observation that the effects of a blade variation will be felt by its adjacent blades in a bladerow and the total influence can be superimposed. Thus, the stochastic influence of the blade variabilities can be estimated using a deterministic model. The observation has been confirmed in both experimental and numerical investigations [6, 20]. As a result, the proposed method can satisfy both the modeling efficiency and accuracy requirement for the blade variability problem.

In the following sections, we will firstly outline the multi-fidelity approach and the influence superposition method. Then, we will apply the method to two test cases of interest to turbomachinery designers: a subsonic low-pressure turbine and a transonic high-pressure turbine. The stagger angle variation will be studied due to its significant impact as noted from the literature. Two specific patterns will be examined: an alternating and a sinusoidal stagger variation pattern. The effects of mis-staggering will be analysed and the accuracy of the new method will be compared against the direct high-fidelity solution.

2. The multi-fidelity influence superposition method

2.1. Method overview

Fig. 1 presents the overview of the combined multi-fidelity influence superposition method to efficiently model the turbine bladerow with stagger angle variation. The method starts with the training stage, where a small number of training sets is required. The data would include both the high-fidelity and low-fidelity calculation of the same training configurations. The high-fidelity results are then projected onto the low-fidelity simulations, creating the sets of source term. Note that the source terms computed in the training stage are the decomposed source terms, which are the individual constituents. In the prediction stage, these source terms can be superposed to approximate an infinite combination of variation patterns and number of blades in the row, given that the amount of mis-staggering is present in the training stage. When combining a superposed source term and a low-fidelity simulation, a multi-fidelity prediction is effectively realized. The proposed methodology combines the accuracy of the high-fidelity simulation and the speed of the low-fidelity simulation. Therefore, the multi-fidelity predictions tend to be both

accurate and fast. Note that the interaction among varied blades will also be captured in the multi-fidelity computations.

In the next sections, the source term-based multi-fidelity method and the influence superposition approach will be described in more details. The objective of the source term-based multi-fidelity method description (section 2.2) is to show that a comparable accuracy of the high-fidelity result can be predicted on the low-fidelity configuration if appropriate source terms are introduced to the equations. On the other hand, the description of the influence superposition approach (section 2.3) shows how a small number of training configurations can be used to approximate the required source terms for a large number of variation patterns.

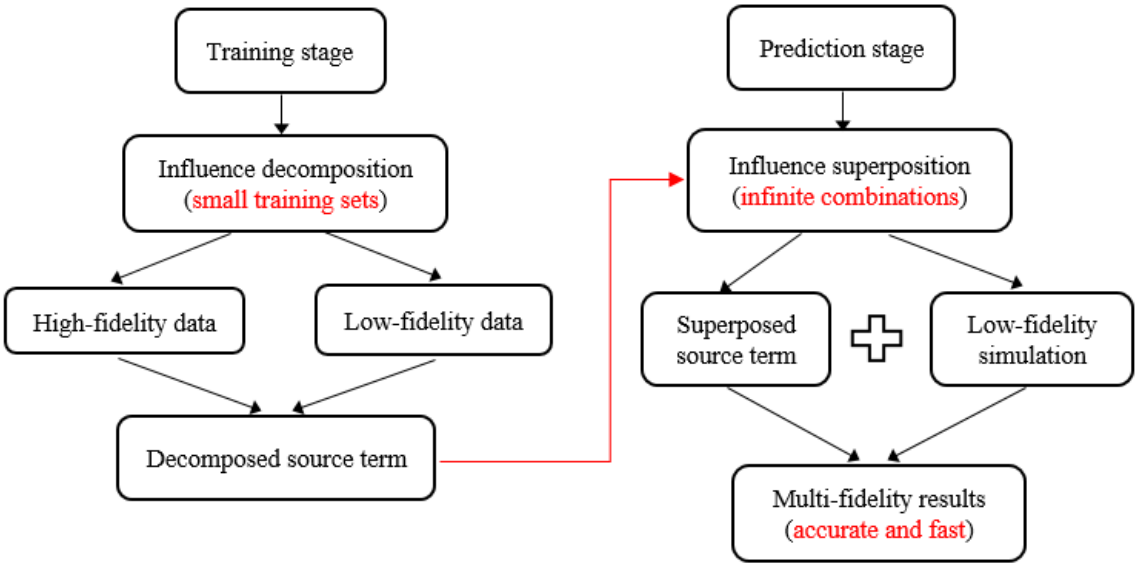

Fig. 1. Overview of the combined multi-fidelity influence superposition method.

2.2. Source term-based multi-fidelity method

The multi-fidelity method used in the present work is the source term-based approach. It stems from the work of He [21, 22], which was developed initially to deal with aero-

thermal problems with disparate length and time scales. The use of this method in the manufacturing variation problems is original. The following section introduces the basis of the source term-based multi-fidelity method.

The governing Navier-Stokes equations for the steady fluid flow can be expressed in a semi-discrete form:

$$R(\boldsymbol{U}) = 0 \tag{1}$$

where $\boldsymbol{U}$ is the conservative flow variables. $R(\boldsymbol{U})$ is the lumped advection and diffusion terms.

We begin with a high-fidelity mesh as in a classical simulation. The mesh is sufficiently fine to resolve all the flow characteristics of interest (e.g. boundary layer, wake, etc.). If the simulation converges, the governing equations are satisfied:

$$R_f(\boldsymbol{U}_f) = 0 \tag{2}$$

Supposing the same flow domain is now discretized with a low-fidelity discretization. The poorly resolved but converged coarse mesh solution still satisfies the equations:

$$R_c(\boldsymbol{U}_c) = 0 \tag{3}$$

The low-fidelity discretization would not predict correctly the flow features having a fine scale that could be obtained otherwise by the high-fidelity computation. Thus, the loss of accuracy by the low-fidelity computation is obvious. However, it is possible to predict the high-fidelity results on a low-fidelity base discretization, which is the objective of the multi-fidelity method.

In order to recover the high-fidelity solution, the solution will be transferred to the low-fidelity discretization through volume-weighted averaging:

$$\boldsymbol{U}_{f\to c} = \frac{1}{\Delta V_c}\sum \boldsymbol{U}_f \Delta V_f \tag{4}$$

where the summation is taken for all the fine mesh cells of volume ΔV_f corresponding to a coarse mesh cell of ΔV_c.

The volume-weighted averaging solution $\boldsymbol{U}_{f\to c}$ to be recovered in the coarse mesh simulation must also satisfy the governing equations. However, due to the difference between the volume-averaged solution $\boldsymbol{U}_{f\to c}$ and the low-fidelity solution $\boldsymbol{U}_c$, the governing equations can only be balanced if a source term is introduced to the right-hand side of the equations:

$$R_c\left(\boldsymbol{U}_{f\to c}\right) \neq 0 \tag{5}$$

$$R_c\left(\boldsymbol{U}_{f\to c}\right) = \boldsymbol{S} \tag{6}$$

where $\boldsymbol{S}$ is the source term arisen due to the difference between the high- and low-fidelity results.

Therefore, it can be concluded that the high-fidelity solution can be predicted on the low-fidelity discretization if an appropriate source term is available to compensate for the errors. Appendix A describes an iterative method to compute the source term in a commercial solver framework. The next section discusses how the influence superposition method can be adopted to estimate the required source term in the context of a mis-staggered turbine bladerow.

2.3. Influence superposition method

Firstly, it should be noted that a change in stagger angle of a reference blade can be felt across the neighbor blades. In light of the superposition theory, the influence of neighbor blades on the reference blade is also the same as that induced by the reference blade onto the neighbor blades. In the current source term-based multi-fidelity framework, the

166 influence is analogous to the source term since both represent the change in flow field.
167 Thus, the superposition theory can be interpreted as:

168 $$\boldsymbol{S}_{total} = \sum_{m=-N/2}^{+N/2} \boldsymbol{S}_m \quad (7)$$

169 where m is the passage number index. N is the number of passages in the multi-passage
170 assembly for which its influence is taken into account. $\boldsymbol{S}_{total}$ is the total source term acting
171 on a reference passage that needs to be approximated to predict the high-fidelity projected
172 solution on the low-fidelity configuration. $\boldsymbol{S}_m$ is the source term contributed from passage
173 index m including the reference passage itself ($m = 0$), the passages in the positive
174 direction ($m = 1,2, \dots, N/2$), and the passages in the negative direction ($m =$
175 $-1, -2, \dots, -N/2$). Note that the positive/negative direction is just the convention for blade
176 numbering and it has no physical meaning in the present work.

177 Eq. 7 states that the total influence felt by the reference blade is the sum of the influence
178 induced by the change in stagger angle of the reference blade itself as well as the neighbor
179 blades. Fig. 2 shows a simple illustration of the superposition principle. On the left hand
180 side, there is the total effects felt by all mis-staggered blades in the row of 3 blades. The
181 uniformly-staggered blades are plotted as black line, while the mis-staggered blades are
182 plotted in red. On the right hand side, it can be seen that the total effects can be decomposed
183 into three separate contributions. In each contribution, only an individual mis-staggered
184 blade is considered, whereas the rest of the bladerow is uniformly-staggered. Three
185 constituent contributions represent the influence of each individual mis-staggered blade.

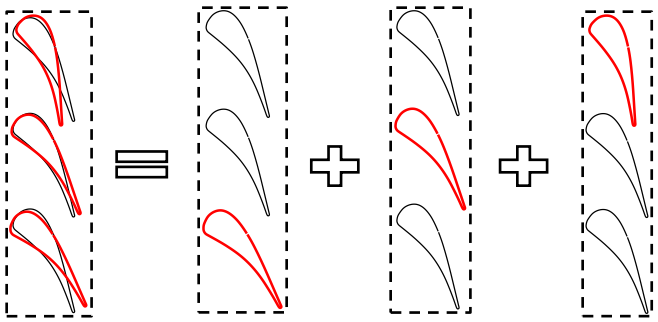

— **uniformly-staggered** — **mis-staggered**

Fig. 2. Superposition principle illustration.

Having understood the basic superposition principle, we will apply this to the source term-based framework. At first, the direct high-fidelity simulation of an ISM truncated-domain needs to be carried out in the pre-computing stage. Notably, only the middle blade is mis-staggered, while the adjacent blades are at the nominal stagger angle as shown in Fig. 3. A five-blade configuration is shown for an illustration purpose. At each re-staggering step of the central blade, the influences on itself and on the adjacent blades are recorded. Then, the ISM truncated-domain high-fidelity flow field solution is volume-weighted averaged and transferred onto the low-fidelity discretization domain. As a result, the source term $\boldsymbol{S}_m$ for an individual blade passage m can be sampled.

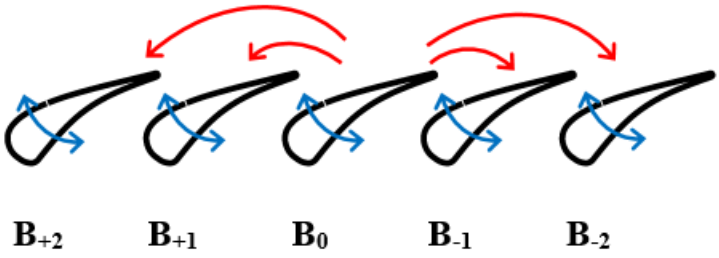

Fig. 3. Source term decomposition method illustration.

Next, in the multi-passage assembly, each blade can be mis-staggered in an irregular pattern. The total source term applied to a reference passage $\boldsymbol{S}_{total}$ is a superposition of each individual passage's source term. Fig. 4 shows the schematic illustration of the source term superposition technique in the mis-staggered bladerow. In this example, only effects of the two closest adjacent blades on each side are shown, in accordance with the way the source term is calculated in the pre-computing stage.

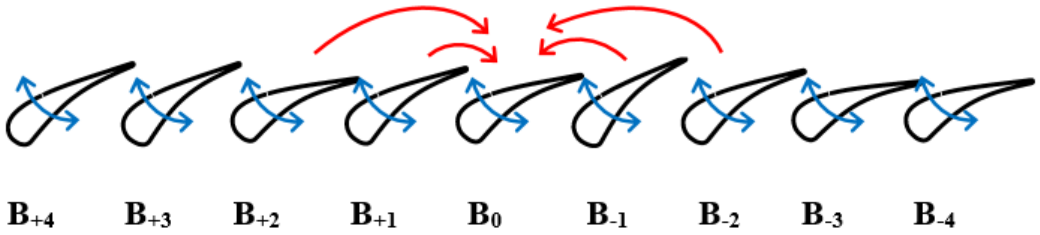

Fig. 4. Source term superimposition method illustration.

Up to this point, it has been clear that the mis-staggering effects can be estimated from a set of deterministic ISM data. Combining the influence superposition method with the multi-fidelity approach thus enables an efficient way to predict the effects of a mis-staggered bladerow. In the rest of the paper, we will apply the newly developed framework to two test cases: a subsonic low-pressure turbine and a transonic high-pressure turbine.

3. Computational setup

3.1. Numerical method

The commercial solver ANSYS CFX is used in the present work. The steady Navier-Stokes equations are solved iteratively in an implicit manner:

$$\nabla \cdot (\rho \boldsymbol{U}) = 0$$

$$\nabla \cdot (\rho \boldsymbol{U} \otimes \boldsymbol{U}) = -\nabla p + \nabla \cdot \tau$$

$$\nabla \cdot (\rho \boldsymbol{U} H) = \nabla \cdot (\lambda \nabla T) + \nabla \cdot (\boldsymbol{U} \cdot \tau) \tag{8}$$

The governing equations represent the conservation of mass, momentum, and energy. In order to close the equations, the Shear Stress Transport (SST) model is adopted. The turbulence model is used with default options. The detailed implementation of the k-omega SST turbulence model is described in the ANSYS theory manual [23].

At the inlet, total pressure, total temperature, and flow angle are specified. Inlet turbulence properties include the turbulence intensity and turbulent length scale. At the outlet, static pressure is used. The solid walls including the blade, hub, and shroud surfaces are modelled as an adiabatic no-slip wall. At two outermost interfaces, a direct periodic condition is applied.

3.2. Meshing

The flow domain is meshed with hexahedral elements. In the high-fidelity mesh, a typical fine mesh for viscous flow simulation is used. The boundary layer is resolved with about 30 elements and the near-wall spacing has $y^+ < 1$. The high-fidelity mesh is also resolved in the wake region. For the transonic test case, attention is paid to the region where the shockwave emanates. On the other hand, the low-fidelity mesh is coarsened in both axial and circumferential direction. In the boundary layer region, there are only few elements with large spacing. Note that the simulation with multi-fidelity method is performed on the low-fidelity mesh. Fig. 5 compares the high- and low-fidelity mesh for the subsonic low-pressure turbine case, whereas Fig. 6 compares that for the transonic high-pressure turbine case.

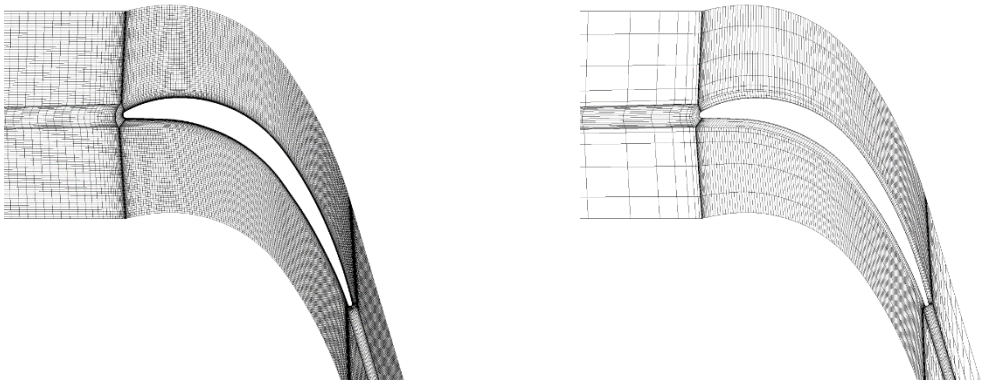

(a) (b)

Fig. 5. Different mesh fidelity configurations for the subsonic LPT test case: (a) High-fidelity mesh; (b) Low-fidelity mesh (also base mesh for multi-fidelity computation).

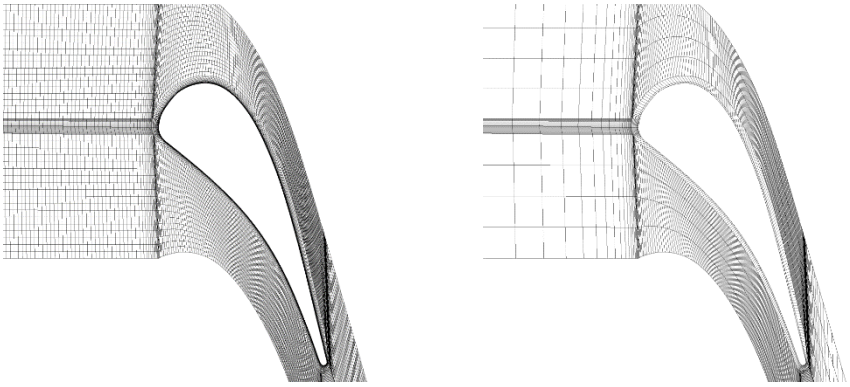

(a) (b)

Fig. 6. Different mesh fidelity configurations for the transonic HPT test case: (a) High-fidelity mesh; (b) Low-fidelity mesh (also base mesh for multi-fidelity computation).

Table 1 summarizes the cell count for different simulation fidelities per two-dimensional blade passage. The total cell count for a given simulation can be scaled accordingly based on the number of passages. It can be seen that both cases can have a reduction factor of one order of magnitude. The lower mesh count can improve the

computing time as well as the flow data storage. Since the multi-fidelity computation is built upon the low-fidelity configuration, this factor also reflects the gain in computational speed for each case.

Table 1 Mesh size comparison per two-dimensional passage.

Case	High-fidelity	Low-fidelity	Reduction factor
Subsonic LPT	30.8k	4.3k	7
Transonic HPT	48.4k	5.3k	9

4. Test case descriptions and validations

4.1. Validation of the subsonic low-pressure turbine

The subsonic low-pressure turbine test case was designed and tested in Durham University [24]. Experiments were performed in a low-speed test facility. Table 2 shows the operating conditions for the LPT test case.

Table 2 Operating conditions for the subsonic low-pressure turbine test case.

Conditions	Experimental	Numerical
Inlet flow angle β_1, deg	0.0	0.0
Reynolds number Re (based on blade chord and exit velocity) $\times 10^5$	2.2	2.21
Isentropic outlet velocity V_{ref}, ms^{-1}	23.2	23.3

Fig. 7 shows the steady pressure on the blade surfaces predicted by the present simulation with different fidelities compared to the experiment for the subsonic LPT test case. The high-fidelity computation is well-matched with the experiment. The low-fidelity

simulation slightly over-predicts the suction surface pressure thus the blade loading. However, it is still in good agreement with the experiment despite of a poor mesh resolution.

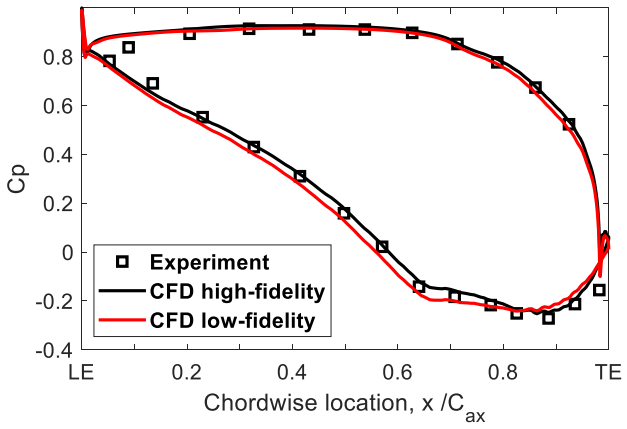

Fig. 7. Steady pressure comparison for LPT test case.

Fig. 8 presents the Mach number contour of the bladerow predicted by the high-fidelity configuration. There is a small separation bubble on the pressure surface at this condition. At off-design condition (negative flow incidence), where the pressure surface separation bubble is expected to grow in size, the difference among computations with various fidelities will be more prominent.

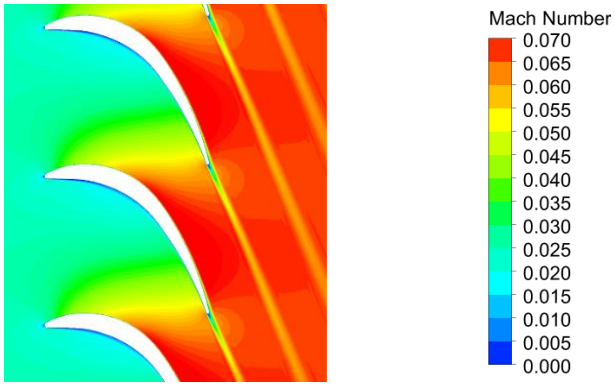

Fig. 8. Mach number contour of the LPT test case.

4.2. Validation of the transonic high-pressure turbine

The transonic high-pressure turbine test case geometry was designed in von Karman Institute [25]. It has been a popular test case for high-pressure turbine aerodynamic and aero-thermal study [25, 26]. The chosen case condition is the MUR47 case. Experiments were performed in the Light Piston Compression Tube facility CT-2, which is a stationary blow-down facility. The test rig comprised of three main parts: a five-meter and one-meter diameter cylinder, the test section and a downstream dump tank. Table 3 compares experimental and numerical operating conditions for the HPT test case.

Table 3 Operating conditions for the transonic high-pressure turbine test case.

Conditions	Experimental	Numerical
Inlet flow angle β_1, deg	0.0	0.0
Reynolds number Re (based on blade chord and exit velocity) $\times 10^6$	1.0	1.13
Isentropic outlet Mach number $M_{2,is}$	1.0200	1.0201

Fig. 9 shows the isentropic Mach number on the blade surfaces predicted by the present simulation with different fidelities compared to the experiment for the transonic HPT test case. The rear part of the suction surface from about 60% chord to the trailing edge is in a transonic flow regime with local Mach number larger than unity. A shockwave is formed on the suction surface around the isentropic Mach number peak at roughly 80% chord. The high-fidelity CFD simulation captures well the location and the strength of the shockwave compared to the experiment. Other RANS computation [27] and the scale-resolved LES computation [28] show a comparable degree of accuracy expected for this test case. On the

other hand, the low-fidelity simulation predicts an erroneous shockwave location, which is about 20% chord upstream compared to the experiment.

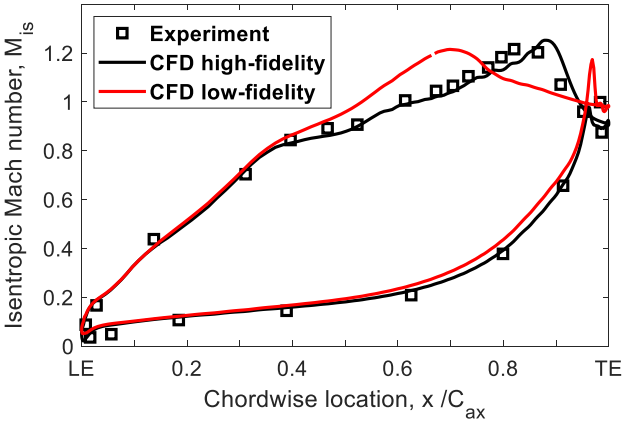

Fig. 9. Isentropic Mach number comparison for the HPT test case.

Fig. 10 presents the Mach number contour of the bladerow predicted by the high-fidelity configuration. The shockwave at 80% chord can be seen, in agreement with the finding using an isentropic Mach number analysis. Moreover, the interaction between shockwaves and wakes of the adjacent blade can also be observed.

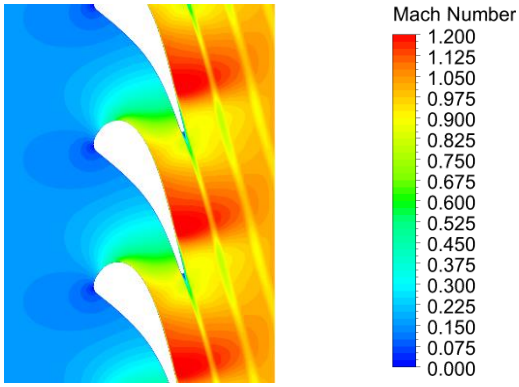

Fig. 10. Mach number contour of the HPT test case.

In order to analyse further the shockwave/wake interaction, we might look at the Schlieren visualization. Fig. 11a shows the Schlieren visualization predicted by the high-fidelity computation, whereas Fig. 11b shows that predicted by the low-fidelity configuration. It is apparent that the shockwave propagation and interaction with wake of the adjacent blade cannot be observed with the low-fidelity computation (note the red circle). Since the high-fidelity Schlieren image is in agreement with that of experiment [25], it can be concluded that the low-fidelity does not only predict an erroneous blade loading but also mask the important flow physics. The under-resolved flow field leads to a wrong prediction of the bladerow's performance.

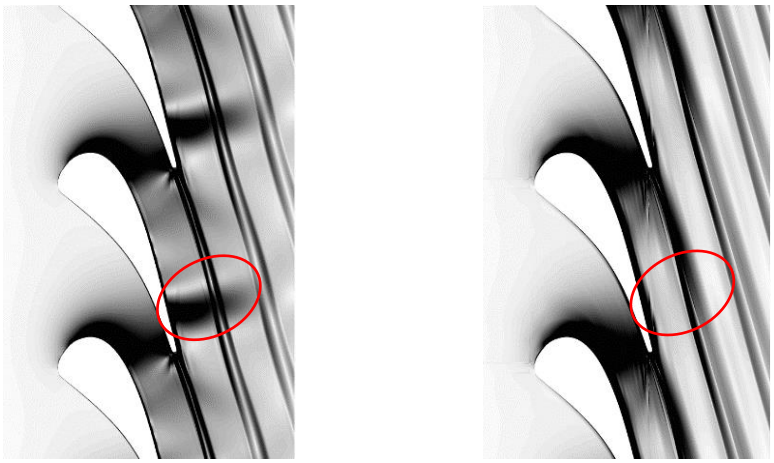

(a) (b)

Fig. 11. Schlieren visualization of the shockwave/wake interaction by different prediction fidelities: (a) High-fidelity; (b) Low-fidelity.

5. Results and discussion

In the main part of the present study, we will apply the combined multi-fidelity approach and influence superposition method to study the effects of mis-stagger angle variations on the bladerow performance. One of the important objective is to assess the

accuracy of the proposed method against the direct high-fidelity simulation results. Two mis-stagger variation pattern will be studied, namely the alternating and sinusoidal pattern. Fig. 12 illustrates the mis-stagger angle variation patterns against the uniform bladerow. The blades are mis-staggered within $\pm 1^0$ from the uniform value. This limit is larger than a typical modern manufacturing uncertainty. However, since variabilities will be amplified during its service life, we use a larger value of deviation to take this into account.

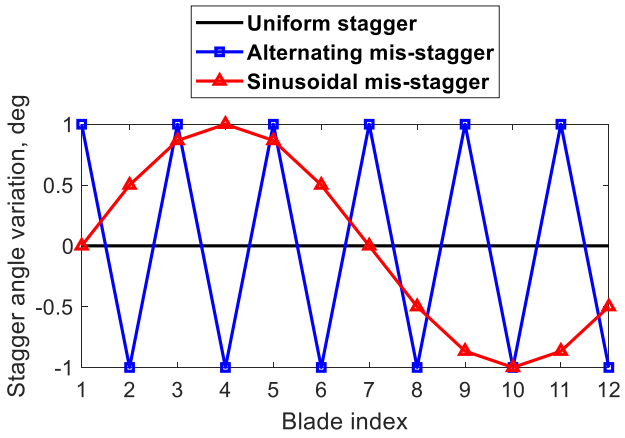

Fig. 12. Stagger angle variation patterns.

5.1. Subsonic low-pressure turbine

5.1.1. Alternating mis-stagger

Fig. 13 shows the steady pressure distribution for the alternating mis-stagger of the low-pressure turbine test case. There are two different responses to alternating mis-stagger depending on the direction of stagger angle change. Fig. 13a presents the pressure distribution for positively mis-staggered blade, whereas Fig. 13b presents that for the negatively mis-staggered blade. In Fig. 13a, the front region near the leading edge on the pressure surface has a lower pressure level. This results in a loss of blade loading in the front part. On the other hand, the front region in Fig. 13b becomes highly loaded with an

increase of pressure level on the pressure surface. In addition, the rear region on the suction surface of Blade 2 (Fig. 13b) has a much flatter pressure distribution. This part is thus prone to separation bubble if the blade loading keeps increasing. More importantly, the multi-fidelity predictions are in good agreement with the high-fidelity simulation results for both blades in the alternatingly mis-staggered LPT case.

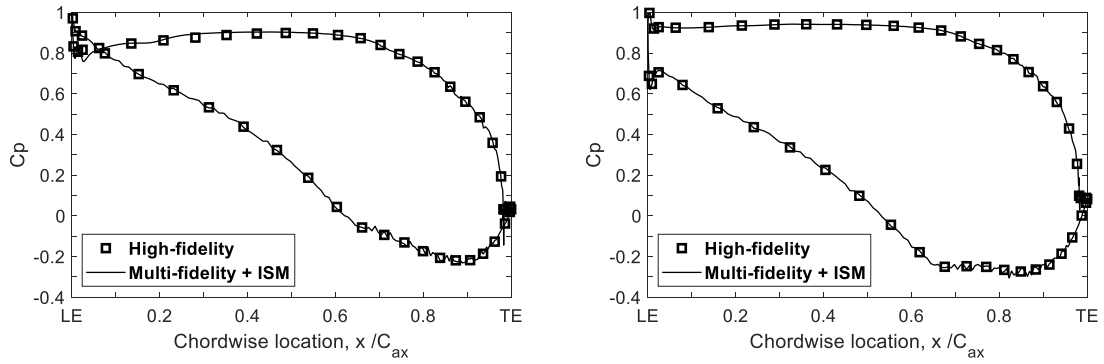

Fig. 13. Steady pressure distribution for the alternating mis-stagger of the subsonic LPT test case: (a) Blade 1 (positively mis-staggered); (b) Blade 2 (negatively mis-staggered).

5.1.2 Sinusoidal mis-stagger

Fig. 14a shows the pressure distribution of the most positively mis-staggered blade of the LPT test case with sinusoidal variation pattern, while Fig. 14b shows that for the most negatively mis-staggered blade. Unlike the previous alternating mis-stagger test case, the pressure distribution changes due to the sinusoidal variation pattern are less significant. This is somewhat expected since the step change in sinusoidal variation pattern is smooth while that in the alternating pattern is more abrupt. Nevertheless, the multi-fidelity predictions of blade loading are in good agreement with the high-fidelity simulation results for both blades in the sinusoidally mis-staggered LPT case.

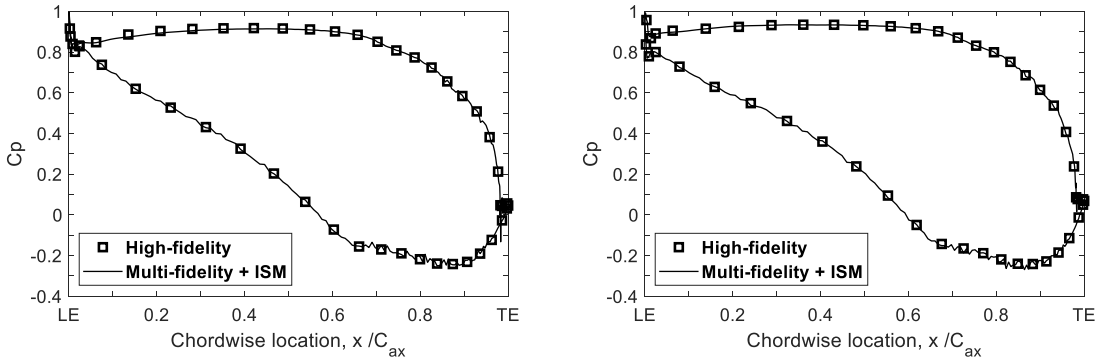

(a) (b)

Fig. 14. Steady pressure distribution for the sinusoidal mis-stagger of the subsonic LPT test case: (a) Blade 4 (most positively mis-staggered); (b) Blade 10 (most negatively mis-staggered).

Fig. 15 presents the flow deflection angle in the circumferential direction. It is apparent the effects of sinusoidal blade mis-staggering propagates further downstream, creating a sinusoidal-like variation in the flow angle distribution. More interestingly, the predictions of multi-fidelity method are well-matched with that of the high-fidelity simulation.

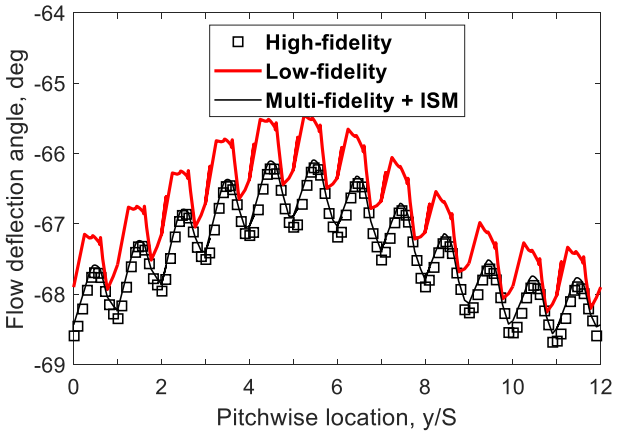

Fig. 15. Exit flow deflection angle of the sinusoidally mis-staggered LPT predicted by different fidelities.

5.1.3. Aerodynamic loss analyses

In this section, we will perform analyses of the low-pressure turbine aerodynamic performance predicted by different modeling fidelities. The aerodynamic loss may come from different sources such as boundary layer loss, trailing edge loss, shock loss (for transonic and supersonic cases), endwall and tip leakage loss (for three-dimensional cases) [29, 30]. To quantify the aerodynamic loss for comparison, we shall use the total pressure loss coefficient as shown in Eq. 9 for a turbine cascade:

$$Y_p = \frac{1}{s}\int_0^s (P_{01} - P_0)/(P_{02} - P_2)\, dy \tag{9}$$

where Y_p is the total pressure loss coefficient. s is the blade pitch. P_{01} is the inlet total pressure. P_{02} is the outlet total pressure. P_2 is the outlet static pressure. P_0 is the total pressure at the traverse plane.

Fig. 16 shows the total pressure loss coefficient predicted by different modeling fidelities. Interestingly, this test case highlights a useful note/observation for the use of the multi-fidelity method in predicting the aerodynamic performance. At the baseline mesh size about 4×10^3 cells, the multi-fidelity method seems to show a significant error compared to the high-fidelity solution. The difference between the high- and multi-fidelity solutions reduces as the mesh is refined. Note that only the mesh in the wake region is refined, we will explain this later when looking at the total pressure profiles. On the other hand, the low-fidelity's total pressure loss coefficient remains almost constant with mesh refinement in the wake region.

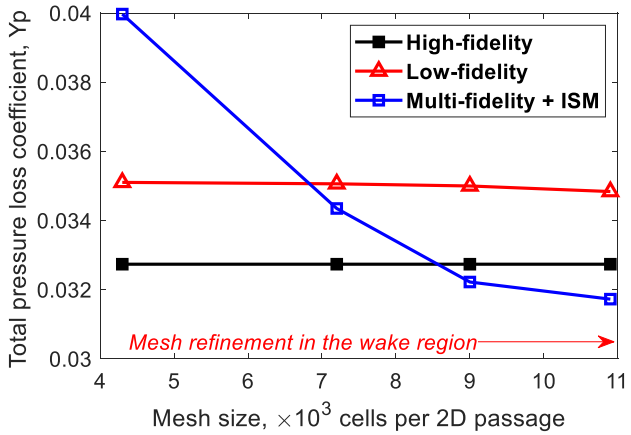

405

406 **Fig. 16.** Total pressure loss coefficient variation with mesh refinement in the wake

407 region.

408

409 Because the total pressure loss coefficient is an averaged quantity, we shall look at the

410 total pressure distribution in the wake region to analyse the underlying reasons behind the

411 discrepancy. Fig. 17a shows the effects of mesh refinement in the wake for the low-fidelity

412 configurations. At the baseline mesh size of 4×10^3 cells, it can be seen that the clustered

413 mesh zone does not coincide with the physical wake core. Instead only a few mesh point

414 is available in the wake core region. To better capture the wake, one can either adjust the

415 mesh such that the mesh is refined in the physical wake core or just simply increase the

416 number of mesh points inside the physical wake core. In this section, we will use the latter

417 method for simplicity to investigate the effects of mesh refinement on the aerodynamic

418 performance predictions by different modeling fidelities. In Fig. 17a, as the mesh is refined,

419 the wake converges to a solution although the converged solution is wrong with a wider

420 wake core and a lower total pressure loss in the wake. This is what we expect because only

421 the wake region mesh is refined and the upstream low-fidelity zones (e.g. under-resolved

422 boundary layer, under-resolved trailing edge) remain similar to the baseline mesh size. On

the other hand, Fig. 17b shows the effects of mesh refinement in the wake for the multi-fidelity configurations. At the baseline mesh size, it is again clear that a few mesh points in the physical wake cannot capture correctly the total pressure deficit, although the multi-fidelity can be seen to be trying to recover the wake shape. Refining the mesh in the wake region has a significant effect on the prediction accuracy of the multi-fidelity method. The improved solution converges to the targeted high-fidelity results.

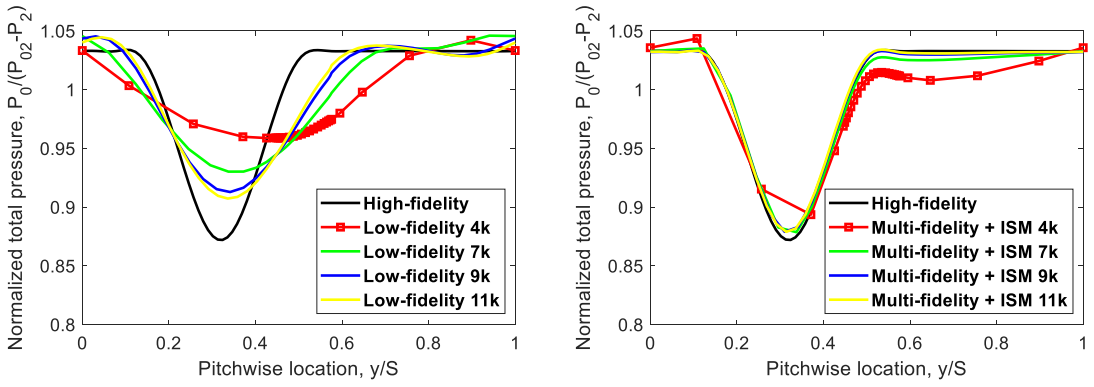

(a) (b)

Fig. 17. Traversed total pressure loss profile with mesh refinement in the wake region across 1 blade pitch: (a) Low-fidelity; (b) Multi-fidelity + ISM.

Combining the findings from Fig. 16 and Fig. 17, we can make some important observations on this interesting test case. About the low-fidelity solutions, although the total pressure loss coefficient at a baseline mesh has a small difference compared to the high-fidelity results, it is due to the wrong reasons. Detailed examination of the total pressure distribution at the traversed plane reveals a significantly erroneous wake profile. Despite refining the mesh in the wake region, the low-fidelity converges to a wrong solution. Regarding the multi-fidelity method, although the total pressure loss coefficient at the baseline mesh has a considerable discrepancy, detailed examination of the total

pressure distribution reveals a qualitatively better wake profile compared to that predicted by the low-fidelity computation. The under-resolved mesh in the physical wake core is found to be responsible for the discrepancy in the multi-fidelity solutions. By simply refining the local mesh in the physical wake core, we can achieve a significant improvement in both qualitative and quantitative comparisons to the high-fidelity solutions.

Because the low-fidelity solution does not present a correct physics mechanism (e.g. wake formation), one should exercise cautious when attempting to use it for aerodynamic investigations. Although the total pressure loss coefficient appears to be good at first sight, it is due to wrong reasons. On the other hand, the multi-fidelity still shows a good capability to reproduce the high-fidelity physical mechanism on the base coarse mesh. This test case also highlights a useful note for future practitioners of the multi-fidelity method: the base coarse mesh should have sufficient mesh points in the regions of interest. One should avoid aggressive coarsening in the regions of interest. It has also been shown that the multi-fidelity has a rapid convergence rate with mesh refinement in high spatial gradient areas.

5.2. Transonic high-pressure turbine

5.2.1. Alternating mis-stagger

Fig. 18 shows the isentropic Mach number distribution for the alternating mis-stagger of the high-pressure turbine test case. Fig. 18a presents the result of the positively mis-staggered blade while Fig. 18b presents that of the negatively mis-staggered blade. The most significant change is observed in the negatively mis-staggered blade (Fig. 18b). The shockwave emanating from this blade has a higher strength, indicating by a higher peak of

Mach number. The low-fidelity simulation always predict erroneous shockwave strength and location for all blades. On the other hand, the multi-fidelity predictions are in good agreement with the high-fidelity simulation results for both blades in the alternatingly mis-staggered HPT case.

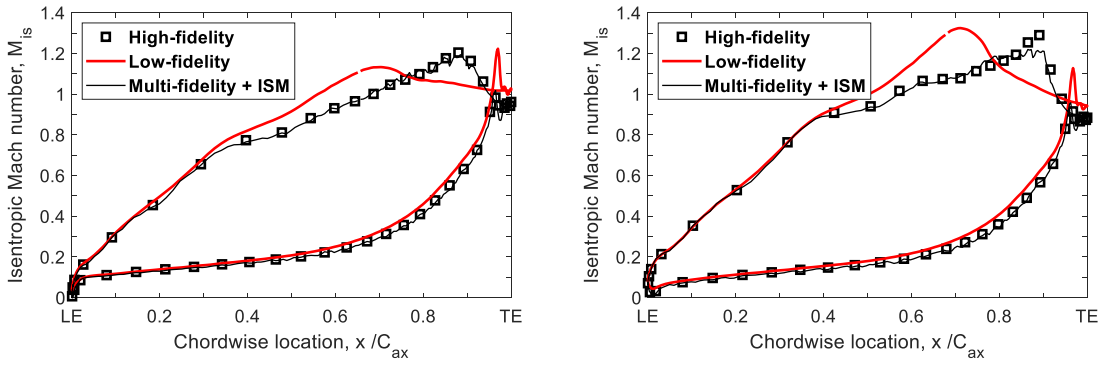

(a) (b)

Fig. 18. Isentropic Mach number distribution for the alternating mis-stagger of the transonic HPT test case: (a) Blade 1 (positively mis-staggered); (b) Blade 2 (negatively mis-staggered).

5.2.2. Sinusoidal mis-stagger

Fig. 19a shows the isentropic Mach number distribution of the most positively mis-staggered blade of the HPT test case with the sinusoidal variation pattern, while Fig. 19b shows that for the most negatively mis-staggered blade. Similarly to the finding from the LPT test case, the changes of blade loading in the sinusoidal variation pattern are less pronounced compared to that in the alternating pattern. The low-fidelity simulation keeps predict erroneous shockwave strength and location for all blades. In contrast, the multi-fidelity predictions are in good agreement with the high-fidelity simulation results for all blades in the sinusoidally mis-staggered HPT case.

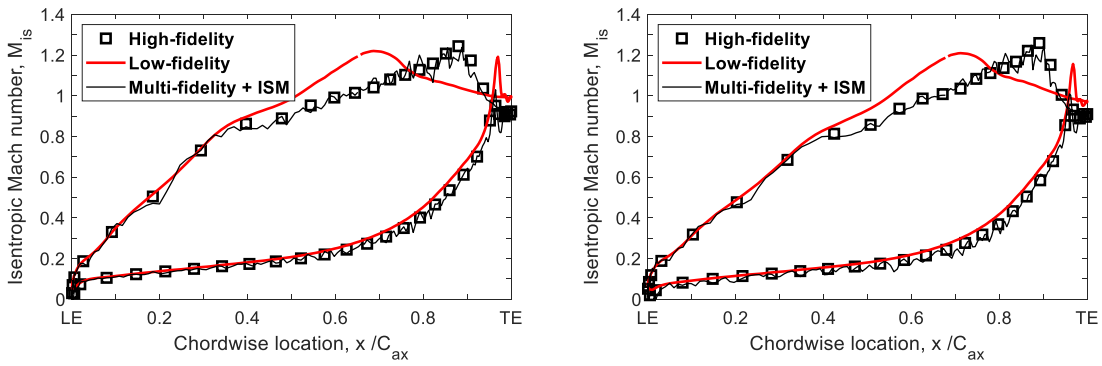

(a) (b)

Fig. 19. Isentropic Mach number distribution for the sinusoidal mis-stagger of the transonic HPT test case: (a) Blade 4 (most positively mis-staggered); (b) Blade 10 (most negatively mis-staggered).

Fig. 20 presents the flow deflection angle in the circumferential direction. Similarly to the LPT case, the effects of mis-staggering propagates further downstream the bladerow, creating a sinusoidal-like variation in the flow angle distribution. The flow angle is significantly affected in the wake region, creating a series of peaks and troughs. However, the magnitude of flow angle variation is much less significant in the low-fidelity simulation results. This finding reinforces the conclusions that the wake mixing and propagation are under-predicted in the low-fidelity simulation. On the other hand, the multi-fidelity simulation shows a good qualitative and quantitative comparison with the high-fidelity simulation.

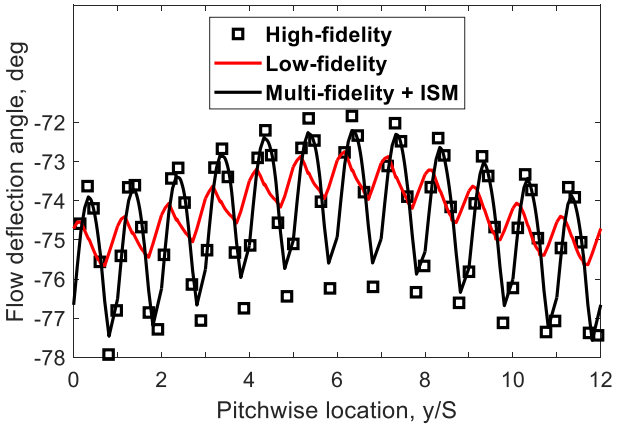

Fig. 20. Exit flow deflection angle of the sinusoidally mis-staggered HPT predicted by different fidelities.

Fig. 21 shows the visualization of local static pressure errors (normalized by the inlet total pressure) between the low- and multi-fidelity simulation in comparison to the reference high-fidelity solution in the sinusoidally mis-staggered HPT test case. The first observation to be made is related to the magnitude of errors. It is clear that the low-fidelity solution has high error level compared to that of the multi-fidelity solution. This finding means that the multi-fidelity solution is closer to the high-fidelity solution compared to the low-fidelity solution. Thus, the multi-fidelity solution has an accuracy that is as good as the direct high-fidelity solution. In addition, another striking observation is the local distribution of errors in the low-fidelity configuration. There are two contrasting zones: one with maximum positive pressure difference and one with maximum negative pressure difference. The 1st zone is on the front region of the suction surface. This corresponds to the location of shockwave formation in the low-fidelity simulation. However, the high-fidelity predicted shockwave does not take place at this region, thus creating a large positive pressure difference (equivalent to negative isentropic Mach number difference,

see Fig. 9 for example). Vice versa, the 2nd zone at the rear part of the suction surface corresponds to the shockwave formation in the high-fidelity simulation. In conclusion, the mismatch of the shockwave location between the high- and low-fidelity simulation is responsible for the alternating pattern of local pressure errors.

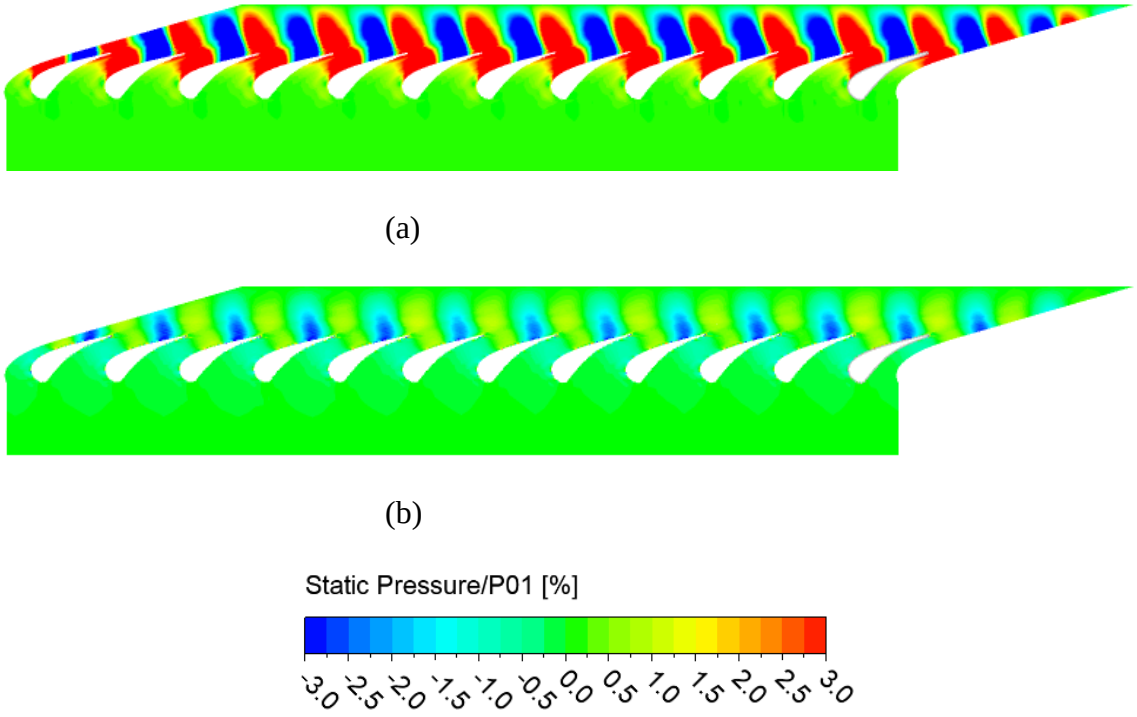

Fig. 21. Static pressure discrepancy (normalized by the inlet total pressure) from the direct high-fidelity solution for: (a) low-fidelity; (b) multi-fidelity computation.

5.2.3. Aerodynamic loss analyses

In this section, we will perform analyses of the high-pressure turbine aerodynamic performance predicted by different modeling fidelities. The total pressure loss coefficient is again used to quantify the aerodynamic loss. Table 4 presents the total pressure loss coefficient calculated at the traversed plane for different modeling configurations. Both the low- and multi-fidelity method overpredicts the total pressure loss coefficient compared to

the high-fidelity solution. However, the low-fidelity computation show a significant error up to 21.6%. The multi-fidelity solution has an improved result with only 6.22% deviation from the targeted high-fidelity solution.

Table 4 Comparison of total pressure loss coefficient predicted by different fidelities.

Configurations	Y_p	Error
High-fidelity	0.0599234	0%
Low-fidelity	0.0728677	+21.6%
Multi-fidelity + ISM	0.0636515	+6.22%

From the previous low-pressure turbine test case, we have learned that the overall loss coefficient might not be a good indicator to judge the success of different modeling fidelities. Thus we need to examine also the total pressure profile at the wake in Fig. 22. Fortunately, the accuracy of the overall loss coefficient is well-reflected in the total pressure distribution in this test case thanks to the correctly clustered mesh in the physical wake core. This finding confirms the capability of the multi-fidelity method for assessing the aerodynamic performance. In addition, it also consolidates the discussion of the mesh requirement in the physical wake core in the previous low-pressure turbine test case.

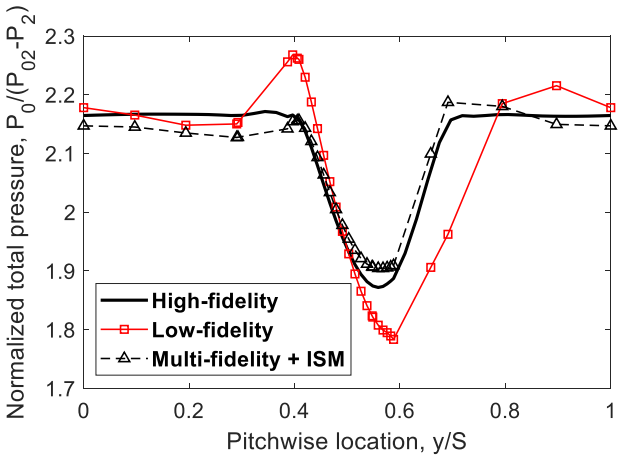

548

549 **Fig. 22.** Traversed total pressure profile across 1 blade pitch predicted by different
550 modeling fidelities.

551

552 **6. Influence decay map**

553 In Section 2, we have mentioned that a five-passage bladerow domain is used in the
554 training stage. It is naturally of interest to ask how the choice of number of training
555 passages would affect the computed source terms. To answer that question, we shall
556 investigate the circumferential distribution of the source terms using a nine-passage
557 domain. All of the steps in the training stage are repeated. Fig. 23 presents the influence
558 map of the x-momentum source terms. It is clear that the source terms decay rapidly in the
559 circumferential direction. Most of the "energy" is contained within a five-passage zone
560 (from B_{+2} to B_{-2}). There is no significant contribution beyond the ±2 passages away from
561 the reference source at the middle. Therefore, it can be concluded that a five-passage
562 domain is sufficient in the training stage. This finding is in line with previous observations
563 in the literature for different applications [6, 20], where the term "influence" represents
564 different kinds of perturbation (e.g. steady and unsteady pressures).

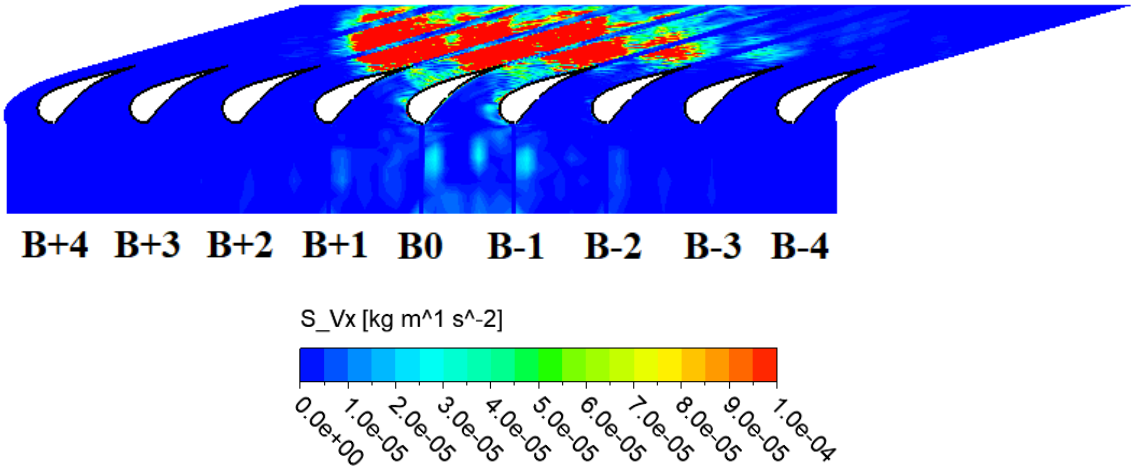

Fig. 23. Influence decay map for the source term amplitudes of the x-momentum equation.

The number of passages used in the training bladerow would affect the training cost and therefore the efficiency of the newly developed method. The observation in this section implies that the passage convergence study should be carried out in the training stage, apart from the conventional mesh convergence study for high-fidelity computations. Fortunately, it has been shown in various applications that typically a few passages are needed thanks to the rapid decay of the influence.

7. Conclusions

Accurate and efficient modeling of the multi-passage blade row with manufacturing variabilities have posed a challenge for the conventional computational method. As the technology boundary is pushed more than ever, the performance prediction of manufacturing variabilities becomes more important. The present work attempts to solve this challenge by proposing a method built upon the framework of both the multi-fidelity approach and the influence superposition method. The combined methodology relies on

584 the superposition of source terms, whose individual constituents have been pre-computed
585 in the training stage. The key enabler is that a small set of configurations is needed in the
586 training stage, while an infinite combination of superposed configurations can be
587 approximated efficiently in the prediction stage. Therefore, the new method has an
588 accuracy level comparable to the direct high-fidelity method, while using a computational
589 resource comparable to the low-fidelity simulation.

590 In the present work, the method has been applied to a subsonic low-pressure turbine
591 and a transonic high-pressure turbine bladerow with alternating and sinusoidal stagger
592 angle variation patterns. The effects of stagger angle variation are summarised below:

593 • Blade loading, aerodynamic loss and exit flow angle are affected by variations
594 of stagger angle.
595 • The mis-staggering effects propagate downstream and create a non-uniform
596 flow field at the bladerow exit, which would affect the downstream bladerow.
597 • Alternating variation pattern has a more pronounced effect compared to
598 sinusoidal pattern.
599

600 In general, the transonic high-pressure turbine case is more sensitive to the simulation
601 fidelity compared to the subsonic low-pressure turbine case. This is due to the high
602 resolution needed to resolve the important flow features in the transonic HPT test case,
603 namely shockwave formation and shockwave/wake interaction. Therefore, the low-fidelity
604 result is not suitable for analysis of manufacturing variabilities if the high-resolution
605 features are important as in this case. For the LPT test case, it has been shown that the
606 overall loss coefficient of the low-fidelity simulation seems to be reasonable at first sight.

However, the detailed investigation of the wake profile reveals that the physical mechanism is poorly predicted.

On the other hand, the multi-fidelity solutions agree both qualitatively and quantitatively to the direct high-fidelity solution. Guidelines on the suitable application of the multi-fidelity method for aerodynamic performance predictions have been discussed. It has been noted that sufficient mesh resolution has to be adopted in the wake region for the multi-fidelity to improve the prediction. Nevertheless, this mesh refinement does not affect significantly the efficiency of the multi-fidelity method due to the rapid convergence rate of the method with mesh refinement. Moreover, the number of passages required at the training stage is also investigated. Thanks to the rapid decay of the influence in the circumferential direction, one would typically need about a five-passage bladerow domain to train the source term. In conclusion, the proposed method has been shown to be successful in providing engineers a tool to explore the variability effects and use it for their blading designs.

Nomenclature

C_p steady pressure coefficient; $C_p = (P - P_2)/(P_{01} - P_2)$

M_{is} isentropic Mach number;

$$M_{is} = \sqrt{\frac{2}{\gamma-1}\left[\left(\frac{P_{01}}{P}\right)^{\gamma-1/\gamma} - 1\right]}$$

P_{01} inlet total pressure, Pa

P_{02} outlet total pressure, Pa

P_2 outlet static pressure, Pa

Y_p	total pressure loss coefficient
HPT	high-pressure turbine
ISM	influence superposition method
LPT	low-pressure turbine
c	low-fidelity
f	high-fidelity
$f \rightarrow c$	multi-fidelity projection
x	axial distance, m
$\boldsymbol{S}$	source term vector
$\boldsymbol{U}$	conservative flow variable vector

Appendix A: Source Term Iterative Computation

Given a high-fidelity and a low-fidelity simulation data, one can find the high-fidelity filtered solution on the low-fidelity representation $\boldsymbol{U}_{f\rightarrow c}$. We know from the theoretical framework of the source term-based multi-fidelity method that a source term $\boldsymbol{S}$ needs to be used to satisfy the governing equations:

$$R_c\left(\boldsymbol{U}_{f\rightarrow c}\right) = \boldsymbol{S} \tag{A1}$$

To compute the source term without knowing the detailed discretization process, we can use an iterative approach. The iteration marches the solution with a pseudo-timestep $\Delta\tau$. After a pseudo-timestep n, the difference between the filtered flow solution and the current flow solution is:

$$\Delta\boldsymbol{S}_n = \frac{1}{\Delta\tau}\left(\boldsymbol{U}_{f\rightarrow c} - \boldsymbol{U}_n\right) \tag{A2}$$

Starting from an initial value of the source term (typically zero), a new value of the source term is updated after each pseudo-timestep. An under-relaxation factor α is used to stabilize the iterative calculation:

$$\boldsymbol{S} = \boldsymbol{S}_{n-1} + \alpha \Delta \boldsymbol{S}_n \tag{A3}$$

The iteration continues until reaching the maximum allowable number of iterations or the L2-norm of the source term change drops below a specified tolerance. It can be easily seen that once $\boldsymbol{U}_n$ approaches $\boldsymbol{U}_{f\to c}$, the source term change $\Delta \boldsymbol{S}_n$ will approach zero and the source term computation is deemed to converge.

References

[1] Xia, Z., Luo, J., and Liu, F., 2019, "Performance Impact of Flow and Geometric Variations for a Turbine Blade Using an Adaptive NIPC Method," *Aerospace Science and Technology, 90,* pp. 127-139. 10.1016/j.ast.2019.04.025

[2] Wang, X., and Zou, Z., 2019, "Uncertainty Analysis of Impact of Geometric Variations on Turbine Blade Performance," *Energy, 176,* pp. 67-80. 10.1016/j.energy.2019.03.140

[3] Yang, J., Xiong, J., McBean, I., Havakechian, S., Liu, F., and Luo, J., 2017, "Performance Impact of Manufacturing Variations for Multistage Steam Turbine," *Journal of Propulsion and Power, 33*(4), pp. 1031-1036. 10.2514/1.B36022

[4] Voigt, P., Högner, L., Fiedler, B., Voigt, M., Mailach, R., Meyer, M., and Nasuf, A., 2019, "Comprehensive Geometric Description of Manufacturing Scatter of High-Pressure Turbine Nozzle Guide Vanes for Probabilistic CFD Analysis," *Journal of Turbomachinery, 142*(8), p. 081002. 10.1115/1.4042892

[5] Lee, W. Y., Dawes, W. N., Coull, J. D., and Goenaga, F., 2019, "The Impact of Manufacturing Variability on Multi-Passage High Pressure Turbine Aerodynamics," AIAA Paper No. 2019-1950. 10.2514/6.2019-1950

[6] Lejon, M., Andersson, N., Ellbrant, L., and Mårtensson, H., 2020, "The Impact of Manufacturing Variations on Performance of a Transonic Axial Compressor Rotor," *Journal of Turbomachinery, 142*(8), p. 081009. 10.1115/1.4046617

[7] Phan, H. M., and He, L., 2021, "Efficient Steady and Unsteady Flow Modeling for Arbitrarily Mis-Staggered Bladerow Under Influence of Inlet Distortion," *Journal of Engineering for Gas Turbines and Power, 143*(7), p. 071009. 10.1115/1.4050364

[8] Phan, H. M., and He, L., 2022, "Investigation of Structurally and Aerodynamically Mistuned Oscillating Cascade Using Fully-Coupled Method," *Journal of Engineering for Gas Turbines and Power, 144*(3), p. 031009. 10.1115/1.4052751

[9] Lange, A., Voigt, M., Vogeler, K., Schrapp, H., Johann, E., and Gümmer, V., 2012, "Impact of Manufacturing Variability and Nonaxisymmetry on High-Pressure Compressor Stage Performance," *Journal of Engineering for Gas Turbines and Power, 134*(3), p. 032504. 10.1115/1.4004404

[10] Koprowski, A., and Rzadkowski, R., 2021, "Computational Fluid Dynamic Analysis of 1MW Steam Turbine Inlet Geometries," *Archives of Thermodynamics, 42*(1), pp. 35-55. 10.24425/ather.2021.136946

[11] He, L., 1997, "Computation of Unsteady Flow Through Steam Turbine Blade Rows at Partial Admission," *Proceedings of the Institution of Mechanical engineers, Part A: Journal of Power and Energy, 211*(3), pp. 197-205. 10.1243/0957650971537105

[12] Li, L. Z., Zhang, J., Luo, X., Yuan, M. N., and Wang, X. M., 2019, "An Aerodynamic ROM of the Blade Subjected to Wake Based on Fourier Method for Flow," *International Journal for Numerical Methods in Fluids, 89*(4-5), pp. 162-179. 10.1002/fld.4687

[13] Zhang, J., Liu, Z., Zhou Li, L., Lu, K., and Ni Yuan, M., 2020, "Aerodynamic Reduced-Order Model of Shape-Change Blade Subjected to Upstream Wake," *Journal of Aerospace Engineering, 33*(5), p. 04020055. 10.1061/(ASCE)AS.1943-5525.0001174

[14] Lee, W. Y., Dawes, W. N., and Coull, J. D., 2021, "The Required Aerodynamic Simulation Fidelity to Usefully Support a Gas Turbine Digital Twin for Manufacturing," *Journal of the Global Power and Propulsion Society, 5*, pp. 15-27. 10.33737/jgpps/132007

[15] Luo, J., Xia, Z., and Liu, F., 2021, "Robust Design Optimization Considering Inlet Flow Angle Variations of a Turbine Cascade," *Aerospace Science and Technology*, *116*, p. 106893. 10.1016/j.ast.2021.106893

[16] Ju, Y., Liu, Y., Jiang, W., and Zhang, C., 2021, "Aerodynamic Analysis and Design Optimization of a Centrifugal Compressor Impeller Considering Realistic Manufacturing Uncertainties," *Aerospace Science and Technology*, *115*, p. 106787. 10.1016/j.ast.2021.106787

[17] Lee, W. Y., Dawes, W. N., and Coull, J. D., 2020, "Physics-Based Part Orientation and Sentencing: A Solution to Manufacturing Variability," *Journal of Turbomachinery*, *142*(10), p. 101001. 10.1115/1.4047613

[18] He, L., 2006, "Fourier Modeling of Steady and Unsteady Nonaxisymmetrical Flows," *Journal of Propulsion and Power*, *22*(1), pp. 197-201. 10.2514/1.15701

[19] Wang, F., and di Mare, L., 2021, "Analysis of Transonic Bladerows with Non-Uniform Geometry Using the Spectral Method," *Journal of Turbomachinery*, *142*(12), p. 121012. 10.1115/1.4051710

[20] Phan, H. M., and He, L., 2020, "Validation Studies of Linear Oscillating Compressor Cascade and Use of Influence Coefficient Method," *Journal of Turbomachinery*, *142*(5), p. 051005. 10.1115/1.4045657

[21] He, L., 2013, "Block-Spectral Mapping for Multi-Scale Solution," *Journal of Computational Physics*, *250*, pp. 13-26. 10.1016/j.jcp.2013.05.004

[22] He, L., 2013, "Fourier Spectral Modelling for Multi-Scale Aero-Thermal Analysis," *International Journal of Computational Fluid Dynamics*, *27*(2), pp. 118-129. 10.1080/10618562.2013.763935

[23] ANSYS CFX 2021 R2, ANSYS CFX – Solver Theory Guide, ANSYS Inc, 2021

[24] Huang, X. Q., He, L., and Bell, D. L., 2009, "Experimental and Computational Study of Oscillating Turbine Cascade and Influence of Part-Span Shrouds," *Journal of Fluids Engineering*, *131*(5), p. 051102. 10.1115/1.3111254

[25] Arts, T., and De Rouvroit, M. L., 1992, "Aero-Thermal Performance of a Two-Dimensional Highly Loaded Transonic Guide Vane: A Test Case for Inviscid and Viscous Flow Computations," *Journal of Turbomachinery*, *114*(1), pp. 147-157. 10.1115/1.2927978

[26] Phan, H. M., Duan, P. H., and Dinh, C. T., 2020, "Numerical Aero-Thermal Study of High-Pressure Turbine Nozzle Guide Vane: Effects of Inflow Conditions," *Physics of Fluids*, *32*(3), p. 034111. 10.1063/1.5144418

[27] S., Vagnoli, 2016, "Assessment of Advanced Numerical Methods for the Aero-Thermal Investigation of Combustor-Turbine Interactions," Ph.D. thesis, University of Florence, Florence, Italy, 2016.

[28] Ito, S., Furukawa, M., Yamada, K., and Manabe, K., 2021, "Applying Ensemble Kalman Filter to Transonic Flows Through a Two-Dimensional Turbine Cascade," *Journal of Fluids Engineering*, *143*(12), p. 121113. 10.1115/1.4052472

[29] Denton, J. D., 1993, "*The 1993 IGTI Scholar Lecture*: Loss Mechanisms in Turbomachines," *Journal of Turbomachinery*, *115*(4), pp. 621-656. 10.1115/1.2929299

[30] Duan, P., Tan, C. S., Scribner, A., and Malandra, A., 2018, "Loss Generation in Transonic Turbine Blading," *Journal of Turbomachinery*, *140*(4), p. 041006. 10.1115/1.4038689